Lawrence Berkeley National Laboratory

LBL Publications

Title
SELF-CONSISTENT PSEUDOPOTENTIAL CALCULATIONS FOR Si(lll) SURFACES: UNRECONSTRUCTED (l x l) and RECONSTRUCTED (2 x l) MODEL STRUCTURES

Permalink
https://escholarship.org/uc/item/3m07c48v

Author
Schluter, M.

Publication Date
1975-06-01

0 0 0 0 4 3 0 5 7 3 0

SELF-CONSISTENT PSEUDOPOTENTIAL CALCULATIONS FOR Si (111) SURFACES: UNRECONSTRUCTED (1 x 1) AND RECONSTRUCTED (2 x 1) MODEL STRUCTURES

M. Schlüter, James R. Chelikowsky, Steven G. Louie, and
Marvin L. Cohen

June 1975

LBL-3944
c.\

DISCLAIMER

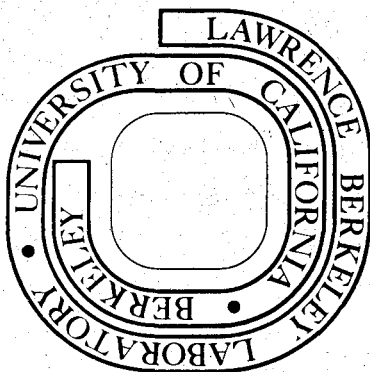Self-consistent Pseudopotential Calculations

for Si (111) Surfaces: Unreconstructed (1 × 1)

and Reconstructed (2 × 1) Model Structures[*]

M. Schlüter,[†] James R. Chelikowsky,

Steven G. Louie[‡] and Marvin L. Cohen

Department of Physics, University of California

and

Inorganic Materials Research Division,

Lawrence Berkeley Laboratory, Berkeley, California 94720

Abstract

A recently developed method involving self-consistent pseudopotentials has been used to calculate the electronic structure of several Si (111) surface models. The results for (1 × 1) unreconstructed, relaxed and unrelaxed surfaces are compared with earlier calculations and discussed in terms of density of states curves and charge density distributions. A fully self-consistent calculation has been carried out for Haneman's (2 × 1) reconstructed surface model. It is found that the important experimental results can be understood using this model, and changes in the electronic structure occurring after reconstruction are rationalized on chemical grounds. In particular infrared absorption measurements, photoemission measurements and recent angular dependent photoemission measurements find consistent explanations.

I. Introduction

In this paper, self-consistent calculations of the electronic structure of several Si (111) surface models are described. The electronic structure of Si (111) surfaces has been investigated in a large number of experimental studies[1-9]. Most of the experiments have been done on surfaces having either (2 × 1) or (7 × 7) superlattice structures which are the metastable and stable surface arrangements of Si (111) respectively. Very useful results, however, have been obtained from theoretical studies on unreconstructed (1 × 1) surface models.[10,11,12,13] In spite of the usefulness of these calculations only results obtained from realistic, reconstructed surface models are consistent with all the experimental data. In the present paper two unreconstructed (1 × 1) surface models (unrelaxed and relaxed) are investigated before studying (for the first time by a self-consistent method) a realistic (2 × 1) reconstructed surface model. We note that self-consistency in the present context means the self-consistent electronic response to a given structural model. Even though calculations of this kind can and have been carried out for several structural models (unrelaxed, relaxed and (2 × 1) reconstructed in our case) it is extremely difficult if not impossible to compare total energies to determine the most favorable surface structural arrangement. The reasons for this are two-fold, first it is known experimentally that the surface geometry is strongly temperature dependent, therefore free energies involving entropies must

be compared. Secondly the total surface energies are large quantities which differ only slightly for the different geometries. With the present techniques they cannot be calculated with sufficient precision to yield reliable results for the energy differences. The present calculations as well as all previously existing self-consistent calculations are therefore restricted to the self-consistent determination of the electronic structure in response to a given structural model.

The only other self-consistent approach to the (111) surface of Si has been presented by Appelbaum and Hamann[10,11] (AH) which like our approach is based on the pseudopotential scheme. For metal

surfaces, pseudopotential calculations by (AH) for Na[14] and by Alldredge and Kleinman (AK) for Al[15] and Li[16] have been carried out very successfully. In addition to the specific problems connected with a self-consistent treatment, the main difficulty arises from the absence of periodicity in treating the surface case.

AH solve this problem by expanding the
electron wavefunction in a mixed representation i.e. two-
dimensional plane waves to account for the periodicity
parallel to the surface multiplied by functions depending
on the remaining spatial coordinate, z, perpendicular to the
surface.   In this mixed representation
the Schrödinger equation   becomes a set of coupled
differential equations in the spatial coordinate, z, which
can be integrated stepwise numerically obeying appropriate
boundary conditions between the vacuum and a matching plane
somewhere in the crystal. Numerical problems and instabilities
however, turn this physically appealing concept into a rather
involved procedure.

AK also start with a mixed representation, however use
a series of analytic trigonometric functions describing the
z-variation of the wavefunction perpendicular to the surface.
Retaining a finite number of these periodic functions is
equivalent to periodically repeating the surface (or better
the thin film). If these films are spaced sufficiently far
enough apart from each other and if they are sufficiently
thick, their surfaces can be regarded as non-interacting and
representative of the true crystal surface. More precisely,
AK expand the z-variation of the wavefunction in a truncated
set of trigonometric sine and $\underset{\Lambda}{\text{cosine}}$ functions which individually
all vanish half way between the films. We believe that these
specific boundary conditions, which are not strictly imposed

by the physics of the system may result in slow convergence behavior since they add an artificial symmetry to the problem.

Our method in contrast to AK's approach uses a set of periodic, trigonometric functions with arbitrary rather than fixed phases.

Using this basis set our procedure is then completely equivalent to placing the film in a periodic array and expanding the wavefunction in plane waves in the usual form as for bulk calculations. The most appealing feature of the approach is that the pseudopotential method (EPM)[17] in its simple standard form can now be applied. In particular, non-local potentials can easily be incorporated (which is not evident in AH's method) and experience e.g. about convergence of wavefunctions gained in calculations of bulk layer crystals[18] can be used. The method adopted for the present study of the electronic structure of Si (111) surfaces however goes beyond the standard EPM through the requirement of self-consistency. As reported in earlier letters[13,19] the method may be applied to various kinds of local configurations like atoms, molecules, impurities, vacancies, one-dimensional chains, two-dimensional layers, surfaces or interfaces. The disadvantages and also the ultimate limitations of the method in dealing with compli-cated systems is connected to the large number of plane waves required to describe the systems' wavefunctions. The use of

symmetry adapted combinations of plane waves is a helpful
tool in dealing with this problem. The remainder of
this paper will be organized as follows. In Section II
the various steps in the self-consistent calculations are
discussed in detail. The results for the electronic structure
of unreconstructed, relaxed and unrelaxed Si (111) surfaces

are presented in Section III. Section IV contains the
discussion of results obtained for a (2 × 1) reconstructed
surface model. In the final Section V the main results are
summarized and some concluding remarks are given.

II. Calculations

In this section a detailed description is given of the
self-consistent calculations, carried out on several Si (111)
surface models. The method has been described briefly
before,[19,13] and mentioned in the introduction of the
present paper. The essence of our method of calculation is
to retain (artificial) periodicity perpendicular to the
surface. In other words a large elongated unit cell is
defined which in two dimensions is spanned by the shortest
lattice vectors parallel to the surface i.e. for the
unreconstructed surface, hexagonal lattice vectors with the
length of $\sqrt{2}/2 \; a_c$, where a_c = 5.43 $\overset{\circ}{A}$ is the lattice constant
of bulk Si (the 2 × 1 reconstructed case will be discussed
later) and by a long c-axis extending over M atomic layers
and N layers of empty space. The numbers M and N have to be
chosen such that (a) the film of material is thick enough
to effectively decouple the two surfaces on each side of
the film and (b) the film surface potential can decay into
the "vacuum" without perturbation arising from other
periodically displaced films. Various test calculations
showed that films of M = 12 atomic layers separated by N ~ 4
layers of empty space resulting in a lattice constant

$c = \frac{5}{2} \sqrt{3} \ a_c$ fulfill these requirements well for Si. The problem thus consists of self-consistently solving the electronic structure of a "periodic" system whose hexagonal unit cell with the above mentioned dimensions contains 12 Si atoms (for the unreconstructed surface). Proceeding in the standard manner we expand the electron wavefunction in plane waves with reciprocal lattice vectors, $\underset{\sim}{G}$:

$$\psi_{\underset{\sim}{k}}^n(\underset{\sim}{r}) = \sum_{\underset{\sim}{G}} a_{\underset{\sim}{k}}^n(\underset{\sim}{G}) e^{i(\underset{\sim}{k}+\underset{\sim}{G}) \cdot \underset{\sim}{r}} \qquad (1)$$

In order to account well for the "structure" in the large unit cell (i.e. the individual atoms or bonds) this expansion has to be carried to sufficiently high $\underset{\sim}{G}$-vectors. A kinetic energy cut-off $E_1 = |\underset{\sim}{G}_{max}|^2 \approx 2.7$ ryd, which is independent of the size of the unit cell was chosen in accordance with earlier bulk calculations[18] on layer crystals. This cutoff which corresponds to a cutoff close to (220) in cubic bulk Si, yields about 160-180 plane waves up to (0,0,12) which allow sufficient variation of the wavefunctions inside the unit cell and at the surface. The variations of the calculated total charge inside the film can be compared to bulk charge densities of Si calculated with much larger cut-off energies. Typical differences are of the order of 20% in the peak values of the charge distribution. To improve the energy convergence another 340 plane waves are included via Löwdin's perturbation scheme[17] which corresponds to a second cutoff at $E_2 = 6.0$ ryd. We would like to mention that the decay of the wavefunction into the "vacuum" does

not represent a particular problem in this context. In fact the wavefunctions at the surface decay into the vacuum over about the same length as do wavefunctions in the bulk of very covalent crystals (e.g. bulk Si or layer compounds) decay along certain (no-bond) directions. This can e.g. be inferred from the results of AH which because they are obtained by real space integration at the surface should be fully converged.

No group theoretical simplifications were incorporated into the present calculations, since it was desirable to solve Schrödinger's equation for general $\underset{\sim}{k}$-points in the two-dimensional (hexagonal) Brillouin zone. The only remaining symmetry operation which would leave these $\underset{\sim}{k}$-points invariant would be a reflection parallel to the surface plane which however is not present in the D_{3d} group of the Si (111) films.

The expansion of the wavefunction leads to a matrix eigenvalue equation of the usual kind

$$\sum_{\underset{\sim}{G}'} (H_{\underset{\sim}{G},\underset{\sim}{G}'} - E\delta_{\underset{\sim}{G},\underset{\sim}{G}'})a_{\underset{\sim}{k}}(\underset{\sim}{G}') = 0 \qquad (2)$$

which is solved by standard methods.[17] The Hamiltonian matrix elements are of the form

$$H_{\underset{\sim}{G},\underset{\sim}{G}'} = |\underset{\sim}{k} + \underset{\sim}{G}|^2 \delta_{\underset{\sim}{G},\underset{\sim}{G}'} + V_{PS}(\underset{\sim}{G},\underset{\sim}{G}') \qquad (3)$$

where $V_{PS}(\underset{\sim}{G},\underset{\sim}{G}')$ represents a general pseudopotential matrix element.

The present calculations are restricted to the use of local pseudopotentials which are known to yield very satis-factory results for bulk Si. The self-consistency loop was entered with an empirical potential

$$V_{emp}(\underset{\sim}{G}) = S(\underset{\sim}{G}) V_{emp}^{at}(|\underset{\sim}{G}|) \qquad (4)$$

where

$$S(\underset{\sim}{G}) = \frac{1}{M} \sum_{\underset{\sim}{\tau_i}}^{M} e^{-i\underset{\sim}{G}\cdot\underset{\sim}{\tau_i}} \qquad (5)$$

is the structure factor describing the atomic positions in the "large" unit cell and where $V_{emp}^{at}(|\underset{\sim}{G}|)$ are form factor values derived from a continuous curve of the form

$$V(q) = \frac{a_1(q^2-a_2)}{\exp[a_3(q^2-a_4)]+1} \qquad (6)$$

The four parameters a_i in Eq. 6 which are given in Table 1 were determined by fitting $V(q)$ to 3 form factor values for bulk Si $V(111) = -0.2241$ ryd, $V(200) = 0.0551$ ryd, $V(311) = 0.0724$ ryd and renormalizing it for the different unit cell volume. Some continuous extrapolation of the kind of Eq. 6 is necessary to obtain form factors for the "new" $\underset{\sim}{G}$-vectors of the surface problem. While the shortest $\underset{\sim}{G}$-vector in bulk Si (111) has the length of 1.06a.u., in the surface problem $\underset{\sim}{G}$-vectors as short as 0.14a.u. are needed. The empirical potential $\underset{\wedge}{\text{Eq. (6)}}$ is very uncertain at these small $\underset{\sim}{G}$-vectors and large changes are expected in the course of self-consistency. The long-range potential fluctuations corresponding to these small $\underset{\sim}{G}$-vectors are absent in a

bulk   Si crystal. In the surface case they are important
as they form the surface potential barrier and strongly
determine work functions and ionization potentials. The
solutions of the eigenvalue problem, Eq. (2), are the energies
$E_n(\underset{\sim}{k})$ and the pseudo wavefunctions defined by Eq. 1. These
quantities were evaluated at 28 $\underset{\sim}{k}$-points in the irreducible
part (1/12) of the two-dimensional hexagonal Brillouin zone.
This relatively large number of sampling points was chosen
rather than one or several "special" $\underset{\sim}{k}$-points to precisely
determine the Fermi level and the total valence charge.
The <u>unreconstructed</u> Si (111) surface is metallic since
  the Fermi level falls within the "dangling bond" surface
band. In this surface band, occupied and unoccupied states
differ in their electronic charge distributions which justifies
the "fine" sampling of the Brillouin zone. In the case of
"true" semiconducting surfaces as unreconstructed (110)
zincblende surfaces or (2 × 1) reconstructed (111) Si surfaces,
we believe calculations based on a few special $\underset{\sim}{k}$-points will
yield good self-consistent results. To determine the Fermi-
level, the density of states, D(E) was evaluated using the
method of Gilat and Dolling[20] with the necessary energy
gradients derived by $\underset{\sim}{k} \cdot \underset{\sim}{p}$ techniques. Once the Fermi level
E_F was known the total valence (pseudo) charge density $\rho(\underset{\sim}{r})$
could be evaluated.

Once the valence charge $\rho(\underset{\sim}{r})$ is known in terms of its Fourier components $\rho(\underset{\sim}{G})$, the Hartree-Fock type screening potentials V_H and V_X can easily be evaluated. V_H is the repulsive Coulomb potential seen by an electron and generated by all the valence electrons. It is defined by Poisson's equation

$$\nabla^2 V_H(\underset{\sim}{r}) = -4\pi e^2 \rho(\underset{\sim}{r}) \tag{7}$$

and it can be written as a Fourier series

$$V_H(\underset{\sim}{r}) = \sum_{\underset{\sim}{G}} V_H(\underset{\sim}{G}) e^{i\underset{\sim}{G}\cdot\underset{\sim}{r}} \tag{8}$$

with

$$V_H(\underset{\sim}{G}) = \frac{4\pi e^2 \rho(\underset{\sim}{G})}{|\underset{\sim}{G}|^2}$$

The divergence of $V_H(\underset{\sim}{G})$ for $|\underset{\sim}{G}| \to 0$ is physically irrelevant since it is exactly cancelled by the ionic potential generated by the positive Si^{+4} ion cores (overall charge neutrality). We can therefore arbitrarily set $V_H(\underset{\sim}{G}=0) = V_{ion}(\underset{\sim}{G}=0) = 0$. Numerically, however, the divergent character of $V_H(\underset{\sim}{G})$ (and $V_{ion}(\underset{\sim}{G})$) for small $\underset{\sim}{G}$-values poses stability problems as we shall discuss later. The non-local Hartree-Fock exchange potential, $V_X(\underset{\sim}{r},\underset{\sim}{r}')$, which if added to the Hartree potential $V_H(\underset{\sim}{r})$ cancels the electron self energy contained in $V_H(\underset{\sim}{r})$, has been approximated using the statis-tical exchange model of Slater.[21] It thus has the local form

$$V_X(\underset{\sim}{r}) = -\alpha 3 e^2 (\frac{3}{8\pi})^{1/3} [\rho(\underset{\sim}{r})]^{1/3} \qquad (9)$$

In the present calculations the value $\alpha = 0.79$ is used in accordance with AH which brings Slater's exchange in agree-ment with Wigner's[22] interpolation formula at the average valence charge density of Si. The function $[\rho(\underset{\sim}{r})]^{1/3}$ has been obtained by evaluating $\rho(\underset{\sim}{r}) = \sum_{\underset{\sim}{G}} \rho(\underset{\sim}{G}) e^{i\underset{\sim}{G} \cdot \underset{\sim}{r}}$ at a three-dimensional grid of $N \sim 10,000$ $\underset{\sim}{r}$-points sampling the real space unit cell. The cube root has then been taken at each individual $\underset{\sim}{r}$-point and the resulting function $[\rho(\underset{\sim}{r})]^{1/3}$ has been transformed back into Fourier space according to

$$\rho^{1/3}(\underset{\sim}{G}) = \frac{1}{N} \sum_{\underset{\sim}{r}_i}^{N} [\rho(\underset{\sim}{r}_i)]^{1/3} e^{-i\underset{\sim}{G} \cdot \underset{\sim}{r}_i} . \qquad (10)$$

The precision of this procedure can easily be tested by omitting the step at which the cube root of $\rho(\underset{\sim}{r}_i)$ is taken. The final $\rho(\underset{\sim}{G})$ should then be identical to the initial values. The exchange potential then has the form

$$V_X(\underset{\sim}{r}) = -\alpha \left[\frac{3}{2\pi}\right] e^2 (3\pi^2)^{1/3} \sum_{\underset{\sim}{G}} \rho^{1/3}(\underset{\sim}{G}) e^{i\underset{\sim}{G}\cdot\underset{\sim}{r}} \qquad (11)$$

The exchange potential is an absolute potential which approaches zero in the vacuum as the charge goes to zero. $\rho^{1/3}(\underset{\sim}{G}{=}0)$ has a finite value and is essential in determining the absolute value of the potential. The sum of the two potentials $V_H(\underset{\sim}{r})$ and $V_X(\underset{\sim}{r})$ yields the electronic screening potential

$$V_{screen}(\underset{\sim}{r}) = \sum_{\underset{\sim}{G}} (V_H(\underset{\sim}{G}){+}V_X(\underset{\sim}{G})) e^{i\underset{\sim}{G}\cdot\underset{\sim}{r}} \qquad (12)$$

and is at each step in the self-consistent loop evaluated from the total valence charge.

After initiating the calculations with an empirical potential V_{emp} (Eq. 4), the self-consistent loop is continued by adding the screening potential V_{screen} to an ionic potential V_{ion} generated by the Si^{+4} ionic cores. This ion pseudo-potential contains in addition to the exchange α, the only parameters of the self-consistent calculation. First, there are the atomic positions in the surface which enter V_{ion} via a structure factor given by Eq. 5. In addition to the structural model, the individual atomic ionic potential is also based on a parametrized model. Assuming that to first order the ion cores do not change in the free ion, in the bulk crystal or in the surface, an atomic model potential which was fit to atomic term values (as done by Heine and Abarenkov[23]) has been used in our calculation. One important (but not sufficient) check on the quality of this potential is to use it to perform a self-consistent Si bulk calculation. This test is not sufficient, since bulk calculations do not

probe the long range Coulomb tail of ionic potentials. In the case of surfaces, however, this tail is of importance. On the other hand, the Coulomb tail is model independent and results in a $1/q^2$ behavior of the Fourier transformed potential for small wavevectors.

The repulsive cores of the ionic model potentials fitted by Heine and Abarenkov to atomic term values are non-local or ℓ-dependent. In the present calculation a local, "on Fermi sphere" approximation was used in deriving the Fourier transform. This Fourier transform was fitted to a four parameter curve of the form

$$V_{ion}^{at}(q) = \frac{a_1}{q^2} [\cos(a_2 q) + a_3] e^{a_4 q^4} . \qquad (13)$$

The values of these four parameters are given in Table 1. The potentials are normalized to an atomic volume of 169 (a.u.)^3 and the units are ryd. if q is entered in a.u. Equation 15 behaves like $1/q^2$ for small q representing the Coulomb tail and decreases exponentially for large q allowing a definition of a reasonable cutoff $q_c \approx 3$ a.u. for Si^{4+}. As mentioned above, self-consistent Si bulk calculations based on this ionic pseudopotential yield a band structure in excellent agreement with the most recent empirical calculations.[24] The most important electronic transition energies are repro- duced to within ± 0.1 eV. The total bulk valence charge derived from this self-consistent bulk calculation compares very favorably with the empirical charge densities of Walter and Cohen.[25] The values of charge densities in the bonds

change from 25.5 to 25.8 electrons per unit cell and at the

atomic sites from 7 to 5.5 which results from a more

repulsive self-consistent potential at the atoms.

The input potentials for steps $\underset{\wedge}{1}$ and 2 of the self-

consistent loop then become

$$V_{in}^{(1)}(\underset{\sim}{r}) = V_{emp}(\underset{\sim}{r})$$

$$V_{in}^{(2)}(\underset{\sim}{r}) = V_{ion}(\underset{\sim}{r}) + V_{screen}^{(1)}(\underset{\sim}{r}) \qquad (14)$$

Note that, while $V_{emp}(\underset{\sim}{r})$ and $V_{ion}(\underset{\sim}{r})$ are linear super-

positions of atomic potentials, all other potentials $V_{screen}^{(n)}$

and $V_{in}^{(n+1)}(n \geq 1)$ are of a more general form and can no

longer be factorized into structure factor times form factor.

This fact accounts for the non-linear nature of the dielectric

screening and results in the existence of "forbidden"

reflections in the self-consistent potential.

Since the potential $V_{emp}(\underset{\sim}{r})$ was determined empirically

for Si bulk crystals, it is not expected to yield a very

good screening charge for a surface described by the ionic

cores $V_{ion}(\underset{\sim}{r})$. In fact $V_{in}^{(2)}(\underset{\sim}{r})$ results in a very different

eigenvalue spectrum and charge than does $V_{in}^{(1)}(\underset{\sim}{r})$ and any

further steps in the self-consistent loop based on a

straightforward extension of Eq. 14 would be unreasonable

and not converge. This very unstable behavior of the self-

consistent potentials in particular for the small G-vectors

has already been described by Lang and Kohn[26] and by AK.[16]

In agreement with these authors we also find that relaxed,

modified versions of Eqs. 14 which compute the input potential

of stage (n+1) from a linear mixture of input and output
potentials of stage (n) does not result in a convenient
method to attain rapid convergence for the surface problem.
In the present calculations these
instabilities were dealt with by computing adjusted input
potentials $V_{in}^{(n)}(G)$ for n > 2 from preceding input and output
potentials individually for each small G-vector. This can
best be done by inspecting V_{out} versus V_{in} graphs separately
for each small G. Even though the various Fourier compo-
nents are not independent, this procedure helps to reach
convergence fairly rapidly. Mathematically the instabilities
are reflected in rather steep curves (with negative slopes)
of V_{out} versus V_{in}, i.e. very small changes in V_{in} result
in large overshoots in V_{out}. For higher G-vectors, $|G| \geq$
la.u., no instabilities occur and convergence is easily
reached. Because of the above mentioned instabilities and
difficulties in determining long range potential fluctuations,
work functions and ionization potentials are   difficult
to obtain correctly by our method.

III.   Results for Unreconstructed Si (111) Surfaces

Clean unreconstructed Si (111) surfaces are known to be
thermodynamically unstable below 900°C.[1] Stability can be
reached at lower temperatures by adsorption of adatoms.[7]
Nevertheless the clean unreconstructed surface presents an
excellent model for the theoretical study of surface effects[10-12]
and results obtained for it can be compared to subsequent
more elaborate (reconstructed) surface calculations. Our
study of the Si (111) surface therefore starts with the
clean, unrelaxed, unreconstructed surface, in which all
surface atoms remain at their exact "bulk" positions. In a
second ("relaxed") model the outermost atomic layer was
rigidly relaxed inwards by an amount of $\Delta = 0.33$ Å as
proposed by AH.[10] In Fig. 1 the crystal structure of Si is
viewed in perspective along the [110] direction. The [111]
direction is vertical. A horizontal (111) surface is obtained
by cutting all vertical bonds in a plane.

An excellent overall impression of the behavior of the
electronic states at the Si (111) surface can be obtained
by considering the total, self-consistent valence charge
distribution, as presented in Fig. 2 for the unrelaxed surface
model. The figure shows charge density contours in a (110)
plane cutting the (111) surface at right angles (see Fig. 1).
The plotting area starts midway between two films and extends
about 4 1/2 atomic layers into the bulk. The atomic
(unrelaxed) positions are indicated by dots. Moving deeper
into the crystal, the charge distribution closely resembles

the Si bulk charge densities; near the surface, it decays

rapidly into the "vacuum". This rapid decay assures the

required "vacuum" and hence the decoupling of the films.

No surface states can be recognized on this plot, since only

a small number of them exists in a continuum of decaying

bulk-like states. It is instructive to compare the charge

distribution deeper inside the crystal to the standard,

highly convergent Si bulk charge densities of Walter and

Cohen.[25] These bulk charge densities which were derived

from wavefunctions including about 90 plane waves up to

$G = (331) 2\pi/a_c$ have values of 25.5, 7 and 11 electrons per

bulk unit cell volume $\Omega = a_c^3/4$ for the bonding site, the

atomic site and the antibonding site respectively. Due to

the lower degree of convergence in the present surface

calculations the charge density reaches values of 20, 9 and

12 at the respective sites. This lack of charge "modula-

tion" which amounts to about 25% at the bonding sites results

in an error in the exchange potential $(\sim \rho^{1/3})$ of at most 8%

at the bonding sites. We believe that this range of

uncertainty in the potential or charge is acceptable and

does not influence the results more than other conceptual

uncertainties like the choice of the factor α scaling Slater's

exchange potential. The total charge density can also be

compared with results obtained by AH for a relaxed Si (111)

surface.[10] (The outermost atomic layer has been relaxed

inwards by 0.33 Å.) Scaling their charge contour plot by

the volume Ω the values 20, 3 and 10 (± 2) are obtained for

the respective sites. Their particularly low value at the atomic site might result from a stronger repulsive core potential.

In Fig. 3 contour plots are presented $\overset{of}{\wedge}$ the self-consistent pseudopotential giving rise to the valence charge discussed above and of the empirical starting potential. The potentials are displayed in the same plane as the charge in Fig. 2, with values given in rydbergs. Self-consistency was reached (within 0.01 Ry) after 5-7 steps. Normalized to approach zero in the vacuum the potential values for the self-consistent and empirical potentials are -1.8 (-1.8) at the bonding site, +0.8 (+0.1) at the atomic site and -1.6 (-1.0)

at the antibonding site respectively. The self-consistent

potential at the bonding sites differs slightly for the

different bonds, thus causing some asymmetries in the bond

charge distributions.   Note   the more

repulsive core of the self-consistent potential resulting

from the model ion potential used. As

mentioned earlier, both potentials lead to very similar bulk

energy spectra and bulk charge densities. The self-

consistent potential of AH for a relaxed surface model

reaches values of around -2.2, >0.2 and -1.6 at the bonding

site, atomic site and antibonding site respectively. This

is in good agreement with our self-consistent potential

except possibly at the atomic site where the AH value is

not explicitly given in ref. 10.

To illustrate the various contributions to the total

self-consistent potential in Fig. 4b, the potentials $V_{ion}(z)$,

$V_H(z)$ and $V_X(z)$ averaged parallel to the surface are plotted

as a function of the coordinate z perpendicular to the surface.

Due to their strong long-range Coulomb character V_{ion} and V_H

show only small short range fluctuations compared to their

absolute values. V_{ion} rises about 30 rydbergs over the last

six atomic layers and forms a strong surface barrier. It is

very delicately balanced by the screening potential V_H

leaving a weak attractive net potential with fluctuations on

the scale of interatomic distances of the order of 0.5 rydbergs.

Strictly speaking only the sum of V_H and V_{ion} is physically meaningful; the individual potentials diverge as $|\underset{\sim}{G}|_{min}^{-2}$.

The sum is added to the exchange potential V_X which is of comparable strength and modulation. The resulting total self-consistent potential is indicated in Fig. 4a. In this figure the original empirical starting potential is superimposed to demonstrate the change in the potential occurring because of the self-consistency procedure. While inside the crystal the two potentials $V_{emp}(z)$ and $V_{SC}(z)$ are almost identical (the potential differences visible in Fig. 3 cancel almost exactly after averaging parallel to the surface), the self-consistent potential $V_{SC}(z)$ is somewhat deeper at the outermost atomic layer and exhibits a higher surface barrier of about 0.2 Ry. These changes localize the charge more in the surface, stabilize the surface states and increase the ionization potential. In fact, using the empirical starting potential, charge originating from states at the top of the valence bands was leaking out into the "vacuum". This charge was confined back to the surface by the stronger potential obtained in course of self-consistency. Though the differences between the empirical and self-consistent surface potentials seem to be relatively small, they are essential to stabilize the surface. An ionization potential of about 4.0 eV has been calculated. As mentioned earlier this quantity is difficult to determine precisely with our method and the calculated value is only approximate (±1 eV).

Figure 5 displays the two-dimensional band structure of a twelve layer Si (111) film based on the self-consistent potential for the relaxed surface model. The band structure is presented for surface k-vectors $\underset{\sim}{k}_{||}$ between

in the hexagonal Brillouin zone
$\Gamma(0,0)$, $M(1/2,0)$, $K(1/3,1/3)$ and $\Gamma(0,0)_{\Lambda}$. The 24 valence
                                                    bulk
bands can be roughly divided into 3_{Λ} groups, representing

the 6 low-lying s-like bands, 6 bands of mixed s- and p-
                                                  separate
character, 11 p-like bands and one$_\Lambda$ p-like dangling-bond

band in the fundamental gap. The three groups of bands,

would with increasing film thickness   approach

continua   separated by several gaps in which most

of the surface states appear. Let us first discuss the

dangling bond bands in the fundamental gap. Suppose a Si

bulk crystal is cut every 12 layers parallel to the (111)

plane and the pieces are gradually separated from each other.

With increasing distance one state each would split away

from both the   valence-bands and the   conduc-

tion bands to meet about at half-gap to form the two fold

degenerate dangling bond surface band corresponding to the

broken bonds on either side of the Si films. In Fig. 5

the two bands are not exactly degenerate corresponding to

some weak interaction (~0.2 eV) still present between opposite

surfaces of the 12 layer films. If the surfaces are un-

relaxed and unreconstructed the two dangling bond bands show

almost no dispersion parallel to the surface, i.e. they would

appear extremely flat in the band structure plot. If the

outermost atomic layer is relaxed inward, the dangling bond

band shows an increased dispersion parallel to the surface
                    slight
together with a$_\Lambda$ overall shift of the bands (see Fig. 5).

This effect shall be discussed later in more detail in

relation to charge densities and densities of states.

In contrast to the dangling bond surface band which exists throughout the two-dimensional Brillouin zone independent of relaxation, other surface states show up only in parts of the two-dimensional Brillouin zone ∧ depend on relaxation. [and some] They are indicated at the high symmetry points Γ, K and M by dots in Fig. 4. A region of particular interest is around the point K. Strongly localized surface states exist in the gap between -7 eV and -9 eV independent of surface relaxation. These states merge into the continuum at M and become strong surface resonances. A similar behavior is found around K between -2 eV and -4 eV. Even though the existence of these surface states does not depend upon relaxation, their exact energy position is a function of relaxation. Other surface states appear only after relaxation like the splitting away of the lowest valence band pair between -9.5 eV and -12.5 eV throughout the zone. All these findings have qualitatively also been obtained in a recent analytical model calculation by Yndurain and Falicov.[27]

Comparison with a tight-binding surface band structure calculated by Pandey and Phillips[12] (PP) shows qualitative agreement, though quantitative differences exist in energy and number of surface states. In particular five surface states are found in our calculations at K which agrees with the calculations of Yndurain and Falicov whereas PP only report four surface states. The existence of more than four surface states at a given vector $k_{\parallel}$ indicates that bonds deeper in the crystal, not connected to the outermost

layer are strongly affected by the surface. The character
of the various surface states will be discussed later in
terms of charge density distributions.

Density of states curves for the self-consistent results
for the unrelaxed and relaxed surface models are presented
in Fig. 6. Since these curves represent the total density
of states for a 12 layer slab, their overall features
strongly resemble those of the Si bulk density of states.
The results for the (2×1) reconstructed surface (insert)
are obtained for a 6 layer slab. They shall be discussed
in the next section together with 12 layer (2×1) reconstructed
surface calculations. To locate structures associated with
surface states (no distinction is made in the present case
between bona fide surface states and strong surface resonances),
we investigated the charge density distributions for small
energy intervals scanning the entire width of the valence
bands. One problem which arises when simulating surfaces
by finite slabs of atoms periodically repeated, is spurious
structure in the density of states due to the "unreal"
periodicity of isolated slabs perpendicular to the surfaces.
Spurious two-dimensional singularities occur. Their number
increases with the number of atomic layers per slab. For the
"true" surface case these singularities become "dense" and
disappear. For finite slab calculations all structures in
the density of states have to be investigated in this spirit.
Similar problems are encountered when simulating an amorphous
material by large unit cells periodically repeated.[28] The

locations of surface states and strong surface resonances
(for the _relaxed_ case) are indicated by arrows in Fig. 6.
Their labelling corresponds to the regions around high
symmetry k-points in the two-dimensional Brillouin zone, from which
they originate   (see dots and labelling in Fig. 5).   The
surface state energies are given in Table 2 and compared
to experimental data obtained from UPS measurements on
(2 × 1) and (7 × 7) reconstructed surfaces.   Also indicated
in Table 2 are the results of the self-consistent pseudo-
potential calculation of AH and of the empirical tight-
binding calculation of PP on unreconstructed relaxed Si
(111) surfaces.

     Let us now examine the various surface bands in more
detail.   When relaxing the outermost atomic layer rigidly
inwards by an amount of $\Delta = 0.33$ Å, a surface band (2-fold
quasi-degenerate in our model originating from the two
surfaces of the slab) throughout the entire zone splits off
between -11 eV and -13 eV.   It essentially corresponds to
s-like states with some p_z admixture centered on the _two_

outermost atomic layers) which decay into the crystal. A typical charge density plot of these surface states near Γ ($\Gamma_{\ell b}$) at about -12.7 eV is shown in Fig. 7 (top). As one follows this surface band from Γ to M to K the charge center moves somewhat back into the crystal, e.g. the charge distribution of the state $K_{\ell b'}$ at about -9.8 eV is mostly s-like on the <u>second</u> atomic layer with charge extending considerably into the "longitudinal" bond between second and third atomic layer. A similar situation is found at M for the state $M_{\ell b'}$ at about -10.7 eV. At these two points (K and M) the predominant s-like charge on the outermost layer is transferred to the surface states $K_{\ell b}$ and $M_{\ell b}$ at somewhat higher energies around -8.5 eV. These states (in particular $K_{\ell b}$) are strongly localized on the outermost layer see Fig. 8 (bottom) and decay into the crystal being localized at every other layer (1,3,5 etc.). Roughly it can therefore be said that at K the state $K_{\ell b'}$ at -9.8 eV has s-like charge on the second, fourth, etc. atomic layer, decaying into the bulk, whereas the state $K_{\ell b}$ at -8.5 eV has decaying s-like charge at the first, third, etc. atomic layer.

The next surface states or strong surface resonances appear only at considerably higher energy and they correspond to mostly p-like states with some s-admixture. Starting at Γ at -1.5 eV (Γ_{tb}) a 2-fold degenerate (4-fold in our case of two surfaces) surface band appears corresponding to the transverse back bonds between first and second atomic layer; its charge distribution is shown in Fig. 7 (bottom).

This band merges into the continuum as one goes from Γ to M where it appears as a strong resonance. Again a region of special interest is at K. A very similar arrangement to

the low lying s-states is found for the energies of the p-states. The bulk-like states merge into two narrow groups of bands separated by a ~2 eV gap (see Fig. 5). One surface state ($K_{\ell b'}$) is found inside this gap at about ~2 eV. In constrast to the s-like surface state $K_{\ell b}$ at -8.5 eV this state does not appear midgap; a small potential perturbation might have moved this more sensitive p-like state slightly up towards the upper group of bulk-like bands. Another surface state (K_{tb}) splits off below the lower group of bulk-like bands at -4.2 eV. The resemblance between the s-like and p-like band structure at K and an inspection of the corresponding charge densities suggest very strong decoupling of s- and p-states at K. This kind of dehybridization decreases band dispersion, localizes states and favors the formation of surface states. In fact it is the special form of the structure factor at K which allows separation into s-states centered on even or odd numbered layers, longitudinal p-states and transverse p-states.[27] To support this statement further we note that the charge distribution for the state K_{tb} at -4.2 eV is almost identical to the charge of the states Γ_{tb} at -1.5 eV (see Fig. 7 bottom) and therefore has strong transverse character appearing between the first and second, third and fourth etc. layer. The state $K_{\ell b'}$ at -2.0 eV (see Fig. 8 top) is of longitudinal character, the charge appears in

the longitudinal bonds between the second and third, fourth

and fifth etc. layer, decaying into the crystal. We would

like to note that the behavior of surface states being

localized at alternating atomic layers is not an artifact

connected with the finite slab approximation; it has analy-

tically been confirmed for semi-infinite surface models.[27]

In contrast to Γ where two transverse back bond states

exist, at K only one such surface state appears, the other

having merged into the continuum. Again the situation at M

is similar to that at K, with smaller gaps, however, and

surface states merging into the continuum. The preceding

analysis showed clearly that surface states can
deeply
"penetrate"$_\Lambda$into the longitudinal bond between second and
restrictions
third layer which puts severe$_\Lambda$on the size of model clusters repre-
senting the surface and which has to be considered in positioning
a matching plane as used by AH separating the surface

region from the bulk. It can be inferred from Fig. 6 that

inward relaxation strengthens the transverse back bonds and

therefore lowers the energies of the states Γ_{tb} and K_{tb}.

It weakens the longitudinal back bonds and raises the energy

of states like $K_{\ell b'}$. These effects are also reflected in

the total charge density. They shall be discussed again in

connection with the (2 × 1) reconstructed surface.

The most prominent surface states are the dangling

bond states in the fundamental gap. In both the un-

relaxed and relaxed cases, the surface bands are

half occupied leaving the surface metallic with a Fermi

level positioned as indicated in Figs. 5 and 6. A charge

density plot for the occupied part of this band is presented

in Fig. 9. The charge originates from states around M and

K and exhibits the very pronounced dangling bond character.

The unoccupied states originate from a region around Γ and

show some stronger mixing with back bond states. Though the

comparative study of the unrelaxed and relaxed surfaces

yields very useful information about the existence energy

positions and energy shifts of surface states, these two
surface models cannot satisfactorily explain a number of
experiments. These experiments include various photo-
emission measurements[29] surface mobility studies,[1] photo-
conductivity[1] and infrared absorption measurements[4] on
freshly cleaved Si (111) surfaces, exhibiting a (2 × 1)
reconstruction. The most important experimental facts which
cannot be explained involve the surface states in and close
to the fundamental gap. To gain some understanding of the
behavior of these states after (2 × 1) reconstruction and
to find explanations for the various experimental results,
we have done fully self-consistent calculations on a (2 × 1)
reconstructed surface model. A detailed discussion of this
surface model and the results obtained is given in the
following section.

IV. Results for a (2 × 1) reconstructed Si (111) surface model

Carefully cleaved clean Si (111) surfaces exhibit a
(2 × 1) superstructure as seen from low energy electron
diffraction (LEED) patterns. At the present time unfortunately
there does not exist a satisfactory analysis of the LEED
intensities which would uniquely determine the (2 × 1)
surface geometry. Any calculation of the electronic struc-
ture of the (2 × 1) surface is therefore necessarily based
on empirical structural models. The situation is complicated
by the fact that the (2 × 1) reconstructed surface is meta-
stable. It transforms into a more complex (7 × 7) structure

upon annealing, which is the thermodynamically stable Si (111) surface geometry, or it transforms into the simple (1 × 1) structure after adsorption of adatoms. Once annealed or contaminated, the (2 × 1) structure cannot be recovered. Due to this fact, models for the metastable (2 × 1) surface cannot easily be established on thermodynamical grounds. Various different reconstruction models have thus been suggested.[8] Most recent discussions seem to favor the formation of the (2 × 1) superstructure by periodically raising and lowering rows of surface atoms leaving a buckled surface. This model for reconstructed surfaces was first suggested in 1961 by Haneman[29] and later developed by Taloni and Haneman.[30] In addition to the periodic raising and lowering of rows of surface atoms, in Haneman's model, the second layer-atoms are slightly shifted laterally to approximately conserve the individual bond lengths of the transverse back bonds between first and second layer. The situation is schematically indicated in Fig. 10. Without the lateral shift of second layer atoms, transverse back bonds of different lengths would exist. This modified Haneman model has recently been proposed by AH.[31] In their model calculations done on two differently relaxed (inward and outward) (1 × 1) surfaces, the main emphasis has been put on the existence of stretched and compressed back bonds. The subsequent discussion of our results obtained for a (2 × 1) Haneman model, however, will show that all essential experimental findings can be understood even if the lengths

of the transverse back bonds are approximately conserved.

The structural parameters entering our (2 × 1) reconstructed surface model are the following: alternating rows of atoms have been raised by 0.18 $\overset{o}{A}$ and lowered by 0.11 $\overset{o}{A}$, $_\wedge$ and second layer atoms have been shifted laterally as indicated by the arrows in Fig. 10 such as to approximately preserve the length of the back bonds. This choice of parameters may not represent an optimum choice. In particular, since these parameters represent an overall outward relaxation of the outermost atomic layer, some surface states which depend on inward relaxation like the states $\Gamma_{\ell b}$ at the bottom of the valence bands will become delocalized. Our main interest in this study however is the behavior of the electronic states in the vicinity of the gap and their dependence on the character of the reconstruction (buckling with preserving the length of back bonds). The planar unit cell now contains 4 atoms. First preliminary calculations have been done on six-layer slabs separated by 3 bond lengths of empty space. The corresponding density of states in the vicinity of the valence band edge, obtained from 72 k-points in the two-dimensional Brillouin zone is shown as an insert in Fig. 6. As expected, qualitative changes compared to the unreconstructed (1 × 1) case occur. Doubling the real space unit cell in one dimension corresponds to folding back the Brillouin zone in certain directions. Thus two surface bands appear separated by a gap resulting from the potential perturbation

of the reconstruction. This behavior is reflected by the density of states in Fig. 6 showing two peaks which now correspond to two different bands. In Fig. 6 the density of states does not vanish between the two peaks, thus leaving the surface semi-metallic. In fact the gap between the two surface bands is comparable or smaller than their dispersion. We believe that this behavior is an artifact of only including 6 layers per slab. The surface states on opposite surfaces of the slab show too much interaction, consequently causing the semimetallic behavior. To obtain more quantitative results (2 × 1) calculations with 12 layers per slab have been performed. Because of the large matrix size (about 320 plane waves were included to obtain the same convergence as for the unreconstructed cases), the self-consistent calculations were based on a two-point scheme ((0,0)Γ and (1/2,1/2)K'). For the final self-consistent potential several $k_{||}$-points along high symmetry directions have also been included. A band structure showing the bands in the vicinity of the fundamental gap is presented in Fig. 11. The two dangling bond surface bands are split by a gap of $\geq$ 0.27 eV throughout the zone. They show some dispersion of only about 0.2 eV. The Fermi-level falls between the two bands, thus creating a semi-conducting surface. To obtain a density of states curve for these bands a four term Fourier expansion for the band energy $E(k_{||})$ has been fitted to the calculated band structure at the four $k_{||}$-points Γ, M', $\tilde{M}$ and K', and subsequently evaluated

over a fine grid of $\underset{\sim}{k}_{||}$-points of the two-
dimensional Brillouin zone. The results are shown in Fig.
12 (bottom). Two structures $\wedge$ separated by about 0.4 eV
                              are found
corresponding $\wedge$ the two surface bands. The lower surface
             to
band which overlaps with states arising from bulk and other

surface bands is centered at about $E = E_V = 0$. Experimental

photoemission data[2,3] show structure at somewhat lower energy

$(E \approx -0.5$ eV). Further lowering of the calculate surface

band and better agreement with experiment can probably be
                       using
obtained by $\wedge$ a different choice of atomic displacement para-

meters. Our results, however, show the definite trend of
                                        combined
splitting the dangling bond surface bands $\wedge$ with an overall lowering

because of the buckling structure.
       Also indicated in Fig.
12 (top) is a joint density of states (JDS) for optical

transitions between the lower and the upper surface bands.
                                       in this plot.
Matrix-element effects have not been considered $\wedge$ The JDS
        qualitatively
curve can be $\wedge$ compared to infrared absorption measurements[4]

(broken line). A quantitative comparison is not reasonable because

of   the ad hoc choice of atomic displacement parameters and
because of probable strong excitonic effects.
It is also instructive to calculate the charge density

distributions for states inside the two peaks in the density

of states of Fig. 12 (bottom). The corresponding charge
                              the
(or hypothetical charge for $\wedge$ unoccupied upper band) is

displayed in Fig. 13 in a (210) plane intersecting the surface

at right angle. This plane corresponds to the (110) plane

of the unreconstructed surface. The buckling raises the

surface atom on the left hand side and lowers the surface

atom on the right hand side. Due to lateral shifts the second layer atoms are slightly moved out of the (210) plane. The states show very interesting real space behavior. Electrons in states originating from the lower peak labelled d_{out} are located predominantly on those atoms which have been raised and avoid those atoms which have been lowered. Conversely the wavefunctions for unoccupied states of the peak labelled d_{in} are concentrated around those atoms which have been lowered. The surface thus exhibits a (2 × 1) pattern of nearly two-fold occupied dangling bond states centered at every second row of atoms. Roughly speaking the unpaired dangling electron of every second surface atom (in) is transferred to its neighboring atom (out) where it pairs up with another electron, thus creating an ionic semi-conducting surface. In view of this picture infrared transitions are expected to have a very weak oscillator strength because of the small wavefunction overlap. In fact, the calculated dipole

matrix elements are of the order of 0.05 $2\pi/a_c$ and about one

order of magnitude smaller than average bulk matrix elements.

However, the net charge transfer obtained in our calculation

is presumably too large and would be decreased by correlation

effects. These effects can be considerable for bands of 0.3 eV

width; since they are not included in our calculations, the

results are of a more qualitative nature. It can be seen from Fig. 13

that the charge distribution of the lower peak (d_{out}) extends

somewhat into the back bonds. This mixing of states happens

around the Γ-point where the lower dangling bond band actually

overlaps with lower lying back bond states. In fact some

of the transverse back bond states (Γ_{tb}) found at -1.5 eV

for the unreconstructed surface rise in energy upon recon-

struction and fall between 0 and -0.8 eV. At $k_{||}$-points

further away from the Γ-point (K', M', $\tilde{M}$) the dangling bond

surface bands have very pure dangling bond character and do

not show any noticeable mixing with the back bonds which

decrease in energy to about -3.5 eV. The existence of
transverse back bonding surface states (or strong surface
resonances) close to the valence band maximum may explain
angular photoemission results[9] involving states between 0
and -1.4 eV. These results show a threefold rotational
pattern as do the transverse back bonding states but
$\overset{\text{do not}}{\wedge}$
the pure longitudinal dangling bond states. The results
we obtained for the (2 × 1) reconstructed surface can be
understood on the basis of simple chemical arguments.
Since our calculations were based on Haneman's model which
excludes   bond length variations (such as AH propose in
their model) the various changes in the electronic structure
must in first order are caused by bond angle variations.
This concept is not new, in fact Haneman's original model
was designed on this basis.

   The following discussion includes three different bonds
and their respective energies i.e. the energies of a state
whose charges are primarily concentrated in one of these
bonds: the (longitudinal) dangling bonds d with energy ε_d,
the transverse back bonds b_t (ε_t) between first and second
atomic layer and the longitudinal back bonds b_ℓ (ε_ℓ) between
second and third atomic layer.

   Let us consider the case of the raised outermost atom.
In this case the bond angles between the longitudinal orbitals
and the transverse orbitals are increased whereas the bond
angles among the transverse orbitals are decreased. The
ideal sp^3 hybridization is consequently changed in such a

way as to increase the amount of s-like character in the longitudinal orbitals and of p-like character in the transverse orbitals. As a consequence the energy ϵ_d of the dangling bonds d is lowered due to an increased s-admixture. The transverse back bonds b_t now contain more p-character which raises their energy ϵ_t and weakens the bonds. The longitudinal back bonds like the dangling bonds contain more s-character which lowers their energy ϵ_ℓ and strengthens them. The inclusion of bond-length variations (AH model) would result in an additional stretching of the transverse back bonds b_t and a further weakening. In the case of the lowered outermost atom the bond angles change the opposite way causing a decrease of s-character in the longitudinal orbitals and an increase of p-character in the transverse orbitals. The energy ϵ_d of the dangling bonds d is raised, the energy ϵ_t of the transverse back bonds b_t is lowered combined with a strengthening of the bonds (an additional bond length contraction would increase this effect) and the energy ϵ_ℓ of the longitudinal back bonds b_ℓ is increased combined with a weakening of the bonds. Raising and lowering of alternating rows of atoms leads in first order to a combination of the above effects. The net effect on the longitudinal back bonds cannot be anticipated in this simple picture. The simple picture apparently underlies our self-consistent pseudopotential results. It accounts for the following facts:

a) the strengthening of the transverse back bonds and the weakening of the longitudinal back bonds in the relaxed (1 × 1) geometry. (Here the transverse back bonds have also been contracted.)

b) the raising of the dangling bond energy ε_b at Γ in the relaxed (1 × 1) geometry.

c) the more s-like character of the lower dangling bond band in the (2 × 1) geometry as compared to the upper more p_z-like dangling bond band. This can be recognized from the dangling bond charge having a different asymmetry around the outermost atoms in Fig. 13 (top and bottom).

d) the localization of the lower occupied dangling bond orbitals on the raised atoms and of the higher unoccupied dangling bond orbitals on the lowered atoms in the (2 × 1) geometry.

e) the raising of the transverse back bond energies ε_t up to about -0.5 eV at Γ and -3.5 at K' for back bonds connected to raised outermost atoms in the (2 × 1) geometry.

V. Conclusions

A recently developed extension[19] of the empirical pseudo-potential method for the self-consistent treatment of local "non-periodic" configurations has been applied to several Si (111) surface models. Three different surface models have been studied including unreconstructed, relaxed and unrelaxed (1 × 1) surfaces which also have been investigated by Appelbaum and Hamann[10] in the only previously existing

self-consistent calculation. Their results are basically
consistent with our calculations. In addition new types
of surface states corresponding to the longitudinal back
bonds between the second and third atomic layer are found
and complete density of states curves are presented. A
buckled (2 × 1) surface model, such as proposed by Haneman
(with preserved back bond lengths) has been used to study
the (2 × 1) reconstructed surface. The salient experimental
results on (2 × 1) Si (111) surfaces can be understood on
the basis of this model. Upon reconstruction, the dangling
bond band is split and lowered considerably in energy. The
surface is found to be semiconducting
        producing an infrared absorption peak at low energies.
Transverse back bonding surface states are found to be
raised in energy and appear between 0 and -0.5 eV below the
valence band edge at Γ and above -3.5 eV at K'. These
        be the origin of the
states may ∧   angular dependent photoemission results
    The various effects are discussed on
chemical grounds in terms of bond angle variations occurring
with reconstruction. Changes in back bond lengths such as
claimed by AH in a recent paper[31] to be _essential_ are thus
not necessary for a satisfactory explanation of spectroscopic
data. The existence of bond length changes, however, cannot
be ruled out on the basis of the existing results since both
bond angle- and bond length variations seem to alter the
electronic structure at the surface in a similar manner.

References

*   Supported in part by the National Science Foundation
Grant DMR72-03206-A02.

†   Swiss National Science Foundation fellow.

†   National Science Foundation graduate fellow.

1. Experimental literature through 1973 is compiled by
   W. Mönch in Festkörperprobleme XIII, 241, (1973).

2. D. E. Eastman and W. D. Grobman, Phys. Rev. Lett. **28**, 1378 (1972).

3. L. F. Wagner and W. E. Spicer, Phys. Rev. Lett. **28**, 1381 (1972).

4. G. Chiarotti, S. Nannarone, R. Pastore and P. Chiaradia, Phys. Rev. **B4**, 3398 (1971).

5. J. E. Rowe and H. Ibach, Phys. Rev. Lett. **31**, 102 (1973).

6. J. E. Rowe and H. Ibach, Phys. Rev. Lett. **32**, 421 (1974).

7. H. Ibach and J. E. Rowe, Surf. Science **43**, 481 (1974).

8. J. E. Rowe and J. C. Phillips, Phys. Rev. Lett. **32**, 1315 (1974).

9. J. E. Rowe, M. M. Traum and N. V. Smith, Phys. Rev. Lett. **33**, 1333 (1974).

10. J. A. Appelbaum and D. R. Hamann, Phys. Rev. Lett. **31**, 106 (1973), Phys. Rev. Lett. **32**, 225 (1974) and Phys. Rev. **B8**, 1777 (1973).

11. S. Ciraci and I. P. Batra (preprint).

12. K. C. Pandey and J. C. Phillips, Phys. Rev. Lett. **32**, 1433 (1974).

13. M. Schlüter, J. R. Chelikowsky, S. G. Louie and M. L. Cohen (to be published); and M. Schlüter, J. R. Chelikowsky and M. L. Cohen (to be published).

14. J. A. Appelbaum and D. R. Hamann, Phys. Rev. $\underline{B6}$, 2166 (1972).

15. G. P. Alldredge and L. Kleinman, Phys. Rev. Lett. $\underline{28}$, 1264 (1972).

16. G. P. Alldredge and L. Kleinman, Phys. Rev. $\underline{B10}$, 559 (1974).

17. M. L. Cohen and V. Heine in Solid State Physics, H. Ehrenreich, F. Seitz and D. Turnbull, eds. (Academic Press, N.Y. 1970), vol. 24, p. 37.

18. E. Mooser, M. Schlüter and I. Ch. Schlüter, J. Phys. Chem. Solids $\underline{35}$, 1269 (1974).

19. M. L. Cohen, M. Schlüter, J. R. Chelikowsky and S. G. Louie (to be published).

20. G. Gilat and G. Dolling, Phys. Lett. $\underline{8}$, 304 (1964).

21. J. C. Slater, Phys. Rev. $\underline{81}$, 385 (1951), W. Kohn and L. J. Sham, Phys. Rev. $\underline{140}$, A1133 (1965).

22. E. P. Wigner, Phys. Rev. $\underline{46}$, 1002 (1934).

23. I. V. Abarenkov and V. Heine, Phil. Mag. $\underline{12}$, 529 (1965).

24. J. R. Chelikowsky and M. L. Cohen, Phys. Rev. $\underline{B10}$, 5095 (1974).

25. J. P. Walter and M. L. Cohen, Phys. Rev. $\underline{B4}$, 1877 (1971).

26. N. D. Lang and W. Kohn, Phys. Rev. $\underline{B1}$, 4555 (1970).

27. L. Falicov and F. Yndurain, J. Phys. C $\underline{8}$, 147 (1975) and ibid. to appear.

28. J. D. Joannopoulos and M. L. Cohen, Phys. Rev. $\underline{B7}$, 2644 (1973).

29. D. Haneman, Phys. Rev. $\underline{121}$, 1093 (1961).

30. A. Taloni and D. Haneman, Surf. Sci. $\underline{10}$, 215 (1968).

31. J. A. Appelbaum and D. Hamann, preprint.

Table Captions

Table 1. Parameters entering Eqs. 6 and 15 to define the empirical and ionic Si pseudopotentials.

Table 2. Calculated energies of surface states and strong surface resonances of the relaxed Si (111) surface at Γ (center), K (corner) and M (edge midpoint) of the two-dimensional Brillouin zone. Also indicated are experimental (UPS) results for (2 × 1) and (7 × 7) reconstructed surfaces. The energy zero is taken at the bulk valence band edge E_V.

Table 1

	V_{emp}^{at}	V_{ion}^{at}
a_1	0.279	-9.917
a_2	2.214	0.791
a_3	0.863	-0.352
a_4	1.535	-0.018

Table 2

	SCLC		AH[e]	PP[f]	experiment	
	(1x1) relaxed surface				(2x1)	(7x7)
Γ	1.2	Γ_d	0.88	1.04		
	-1.5(2x)	Γ_{tb}	-1.95(2x)	-1.71(2x)	~-1.0[d]	-1.5[a]
	-12.7	Γ_{Lb}	-12.87	-12.9	-11.7[a]	-12.3[a]
K	0.5	K_d		0.11	-0.5[a] -0.45[b] -0.6[c]	0.1[a]
	-2.0	$K_{Lb'}$				
	-4.2	K_{tb}		-5.65		
	-8.5	K_{Lb}		-8.35		-7.5[a]
	-9.8	$K_{Lb'}$		-9.6		
M	0.5	M_d	0.04	0.17		
	-2.6	$M_{\ell b'}$				
	-3.1	M_{tb}	-3.55	-3.78		-3.6[a]
	-8.1 } -8.7	M_{Lb}				
	-10.7	$M_{Lb'}$				

a) ref. 6; b) ref. 2; c) ref. 3; d) ref. 9; e) ref. 10; f) ref. 12

Figure Captions

Fig. 1. Perspective view of the Si crystal structure
projected on a (110) plane. The [111] direction is
vertical. The (111) surface is obtained by cutting
the vertical bonds in a$_\Lambda$ plane. $\overset{\text{horizontal}}{}$

Fig. 2. Total valence charge distribution for an unrelaxed
Si (111) surface. The charge is plotted as contours
in a (110) plane intersecting the (111) surface at
right angles. The plotting area starts in the vacuum
and extends about $4\frac{1}{2}$ atomic layers into the crystal.
The atomic positions and bond directions are indicated
by dots and heavy lines respectively. The contours
are normalized to electrons per Si bulk unit cell
volume $\Omega_0 = \dfrac{a_c{}^3}{4}$.

Fig. 3. Contour plots of the empirical starting potential
V_{emp} (top) and the final self-consistent potential V_{SC}
(bottom). The plotting areas are identical to Fig. 2.
The potential values are given in rydbergs normalized
to zero in the vacuum.

Fig. 4a. Empirical (V_{emp}) and self-consistent (V_{SC}) potentials
averaged parallel to the (111) surface plotted as a
function of the coordinate z perpendicular to the surface.
b. Individual potential contributions adding up to the
self-consistent potential V_{SC} of Fig. 4a.

Fig. 5. Two-dimensional band structure of a twelve layer
Si (111) film (relaxed surface model). The energy is
plotted as a function of $\underset{\sim}{k}_{||}$ in the two-dimensional

hexagonal Brillouin zone. The various surface states or strong surface resonances at high symmetry points are indicated by dots and labelled according to the description in the text.

Fig. 6. Density of states curves for the self-consistent results on twelve layer films for the relaxed (broken line) and unrelaxed (solid line) surface geometry. Surface states are indicated by arrows and labelled according to Fig. 5. Inserted is the density of states in the vicinity of the fundamental gap for a six layer (2×1) reconstructed surface model.

Fig. 7. Charge density contour plots for two surface states at Γ. The states (Γ_{Lb}) at -12.7 eV form the bottom of the valence bands (top figure), the transverse back bonds Γ_{tb} (bottom figure) are located -1.5 eV below the valence band maximum. The indicated charge values are only for comparison.

Fig. 8. Charge density contour plots for two surface states at K. The longitudinal p-like back bond orbitals $K_{\ell b'}$ (top figure) are located at -2 eV while the s-like charge $K_{\ell b}$ localized on the outermost, third, etc. atomic layers (bottom figure) has an energy of -8.5 eV.

Fig. 9. Charge density contour plot of the dangling bond state K_d at 0.5 eV around the points M and K in the Brillouin zone.

Fig. 10. Schematic representation of the ideal and (2×1) reconstructed Si (111) surface. The reconstruction is

done according to Haneman's model[23] and leaves the
surface buckled as indicated by arrows. The slight
lateral shifts of second layer atoms are also indicated
by arrows.

Fig. 11. Two-dimensional band structure around the fundamental
gap for a (2 × 1) reconstructed Si (111) twelve layer
film. The folded back Brillouin zone is indicated in
the insert.

Fig. 12. Calculated joint density of states curve for low
energy transitions between dangling bond bands of (2 × 1)
Si (111) (top). Also indicated is the experimental
absorption $\epsilon_2(\omega)$ as obtained in Ref. 4. The bottom
figure shows the regular density of states for the two
dangling bond bands (d_{in} and d_{out}) of (2 × 1) Si (111).

Fig. 13. Charge density contour plots for the dangling bond
states d_{out}(top) and d_{in} (bottom) of 2 × 1) Si (111).
The charge is plotted in a (210) plane of (2 × 1) Si
which corresponds to the (110) plane of (1 × 1) Si. The
raised and lowered atoms are marked by arrows.
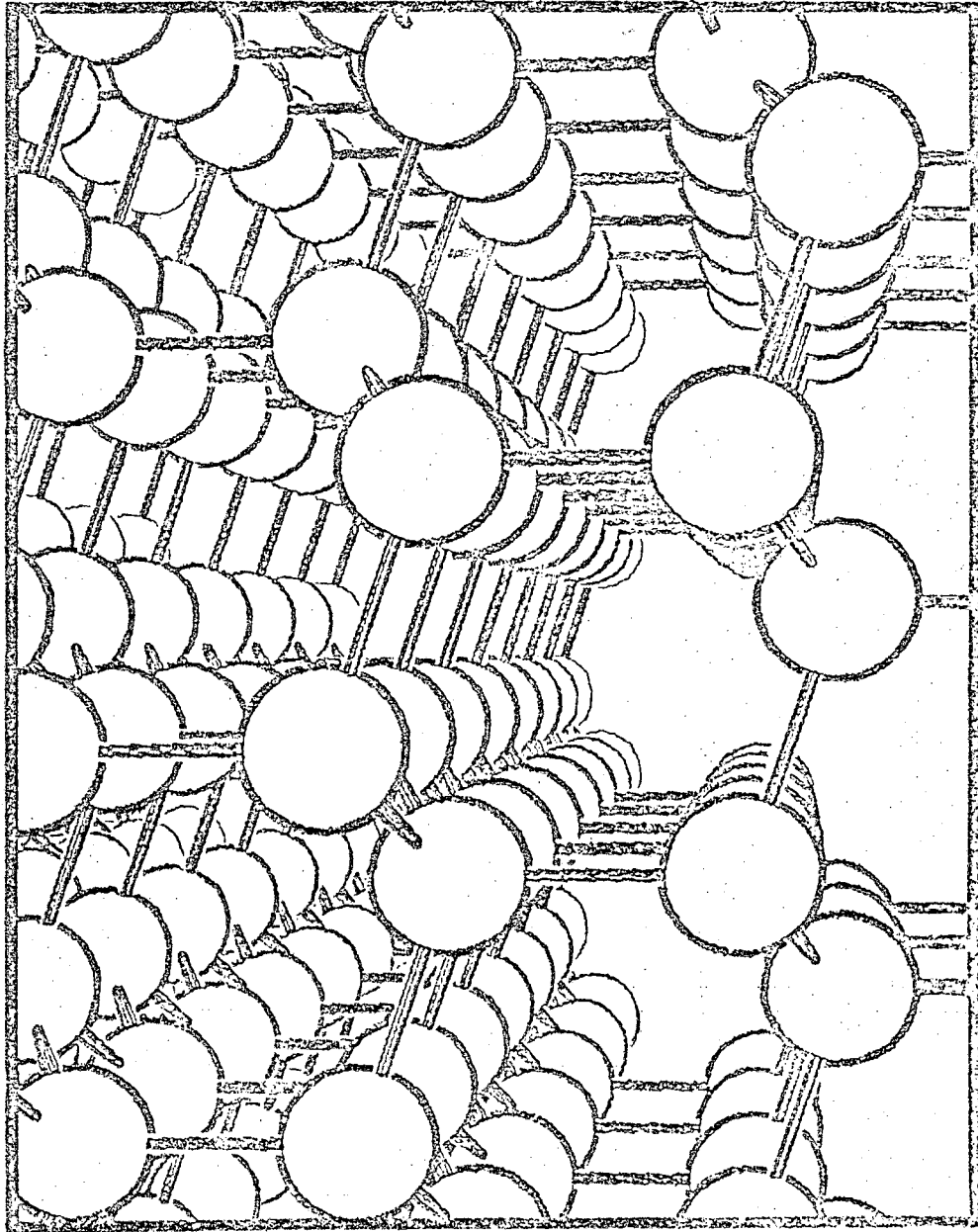
Figure 1

Si (111) SURFACE, UNRELAXED
TOTAL VALENCE CHARGE

Figure 2

Si (111) SURFACE, UNRELAXED
V_{emp} (Ry)

Si (111) SURFACE, UNRELAXED
V_{sc} (Ry)
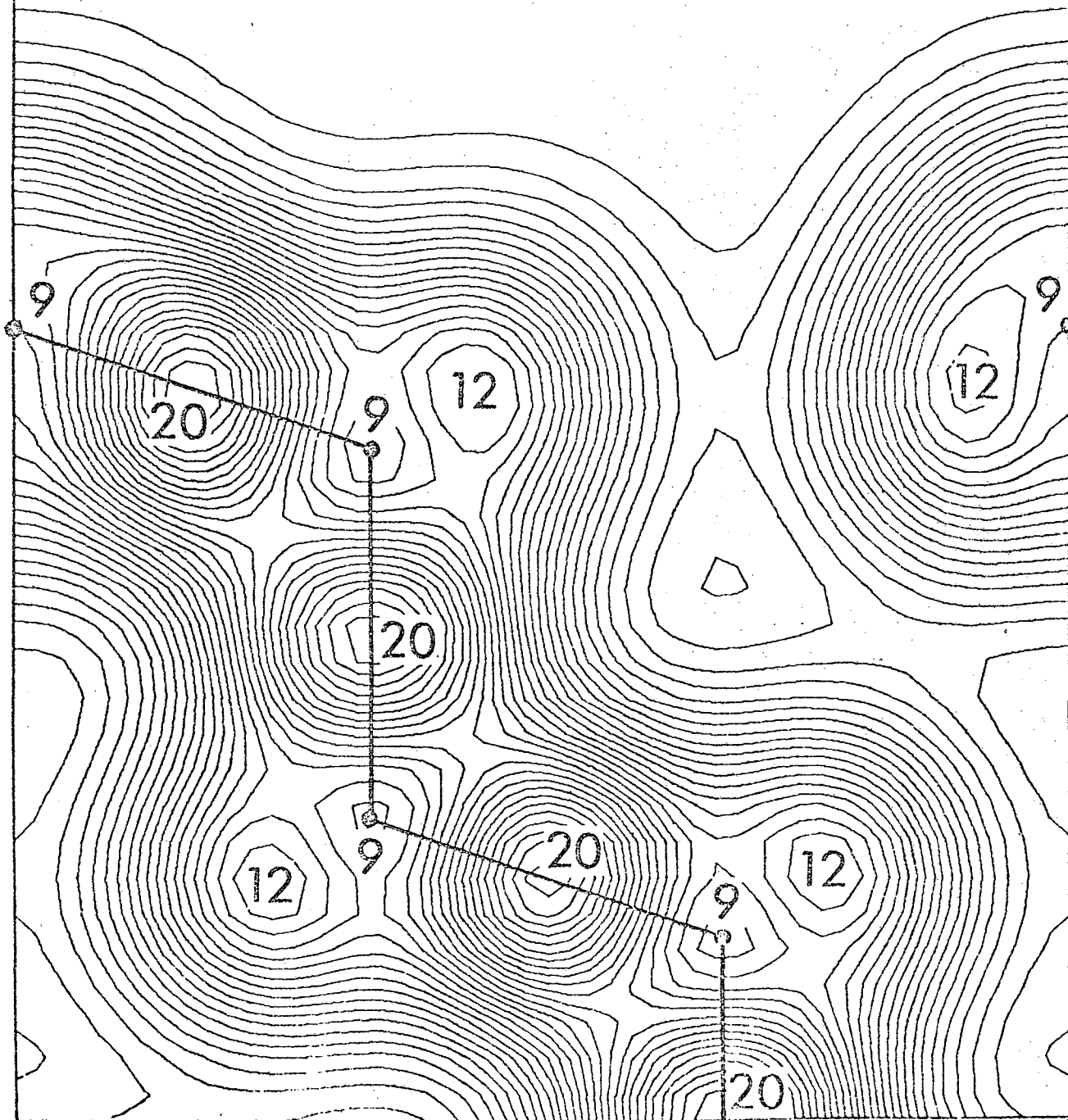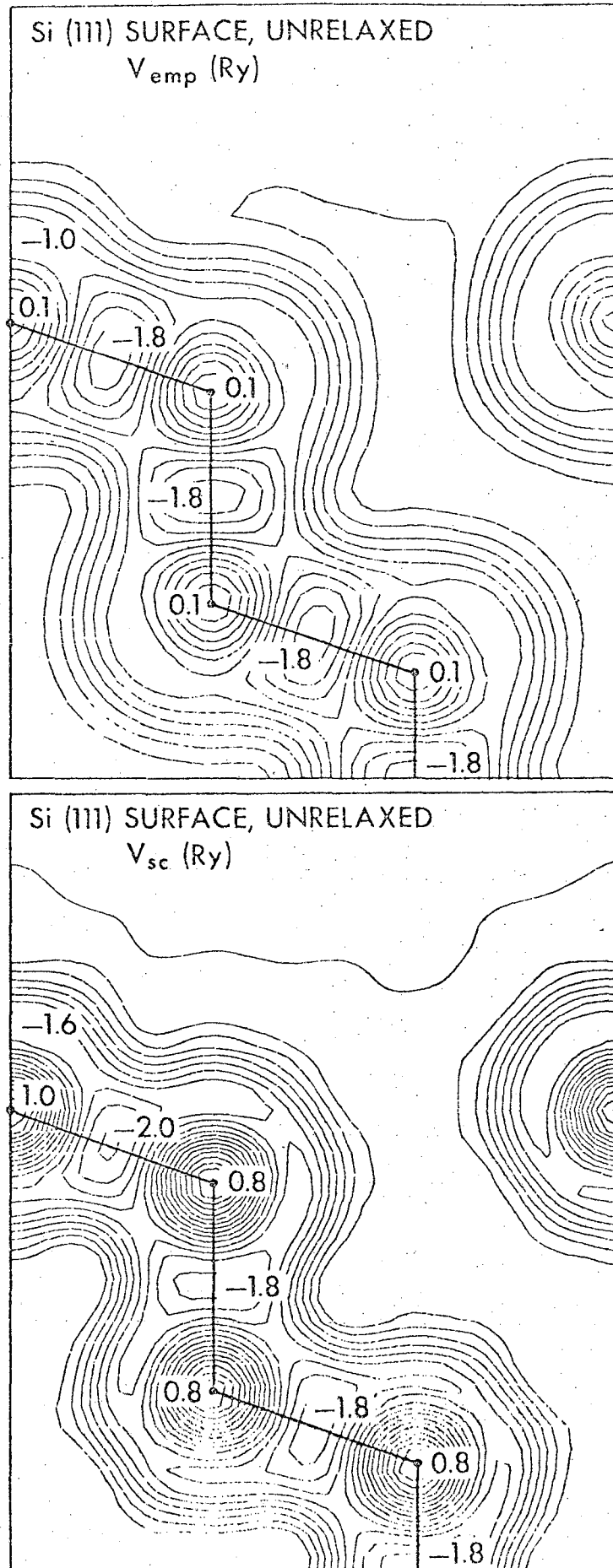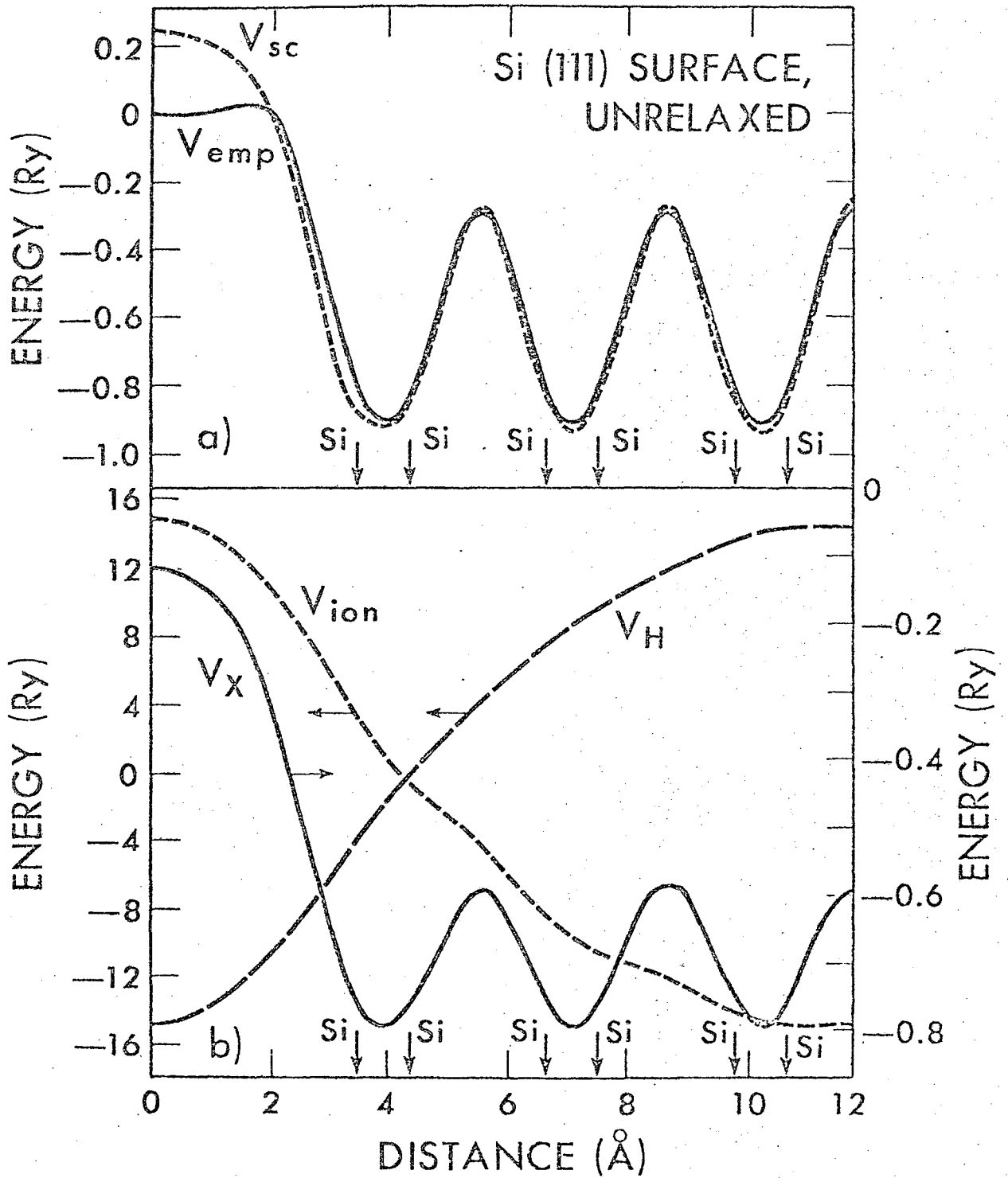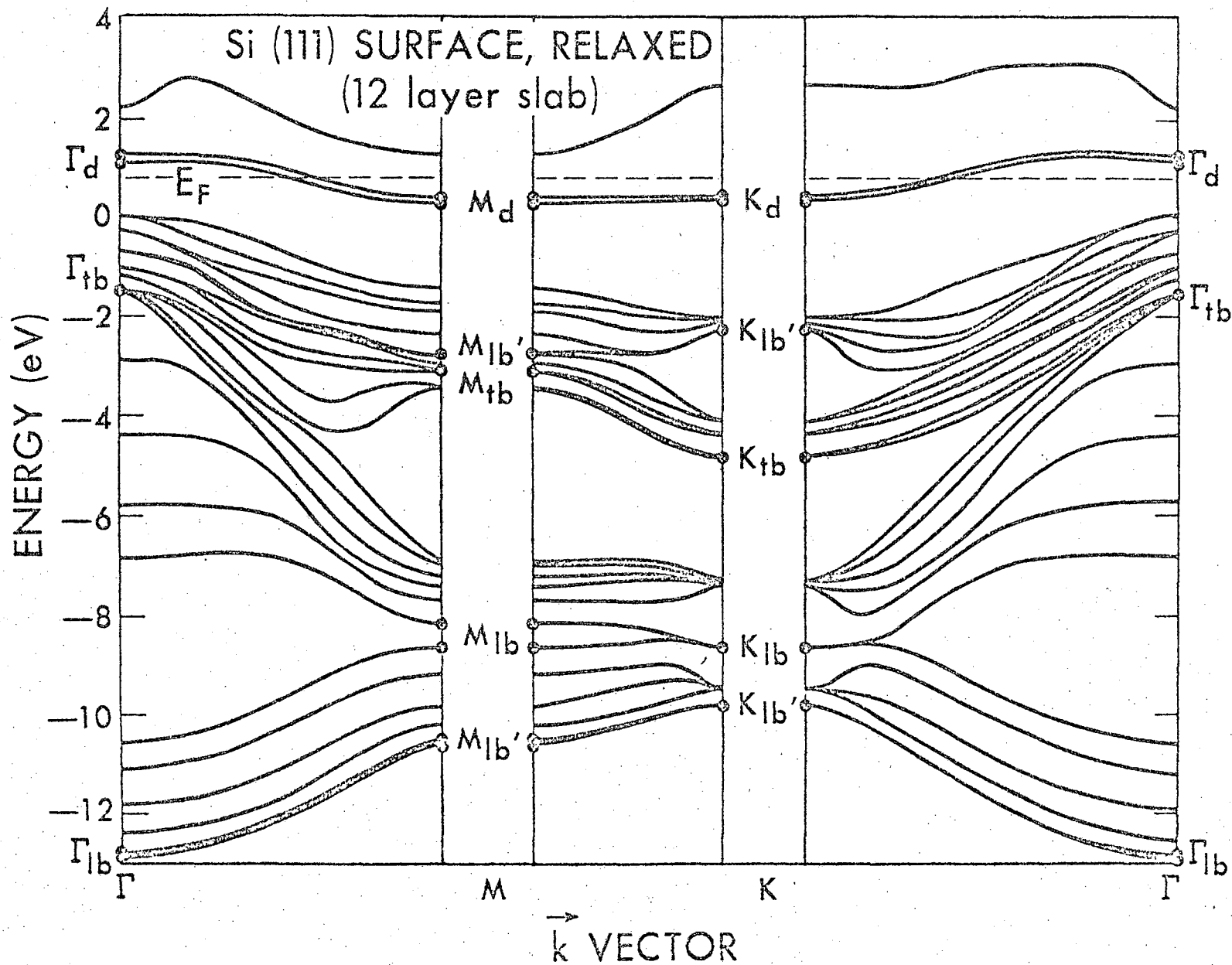
Figure 3

Figure 4

Figure 5
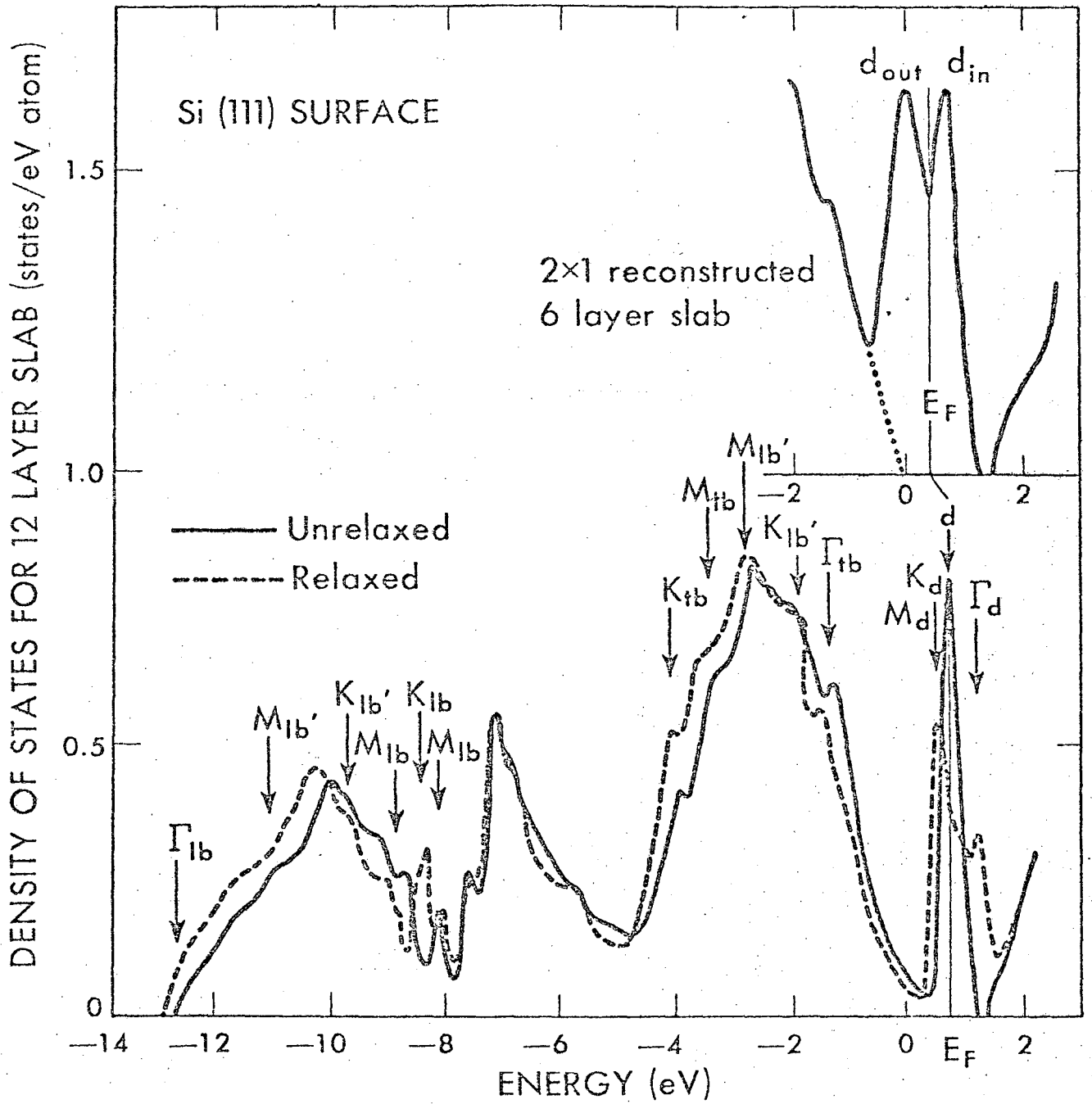
Figure 6

Si (111) SURFACE, RELAXED STATES NEAR BOTTOM OF VALENCE BAND AT −12.7 eV (Γ_{lb})
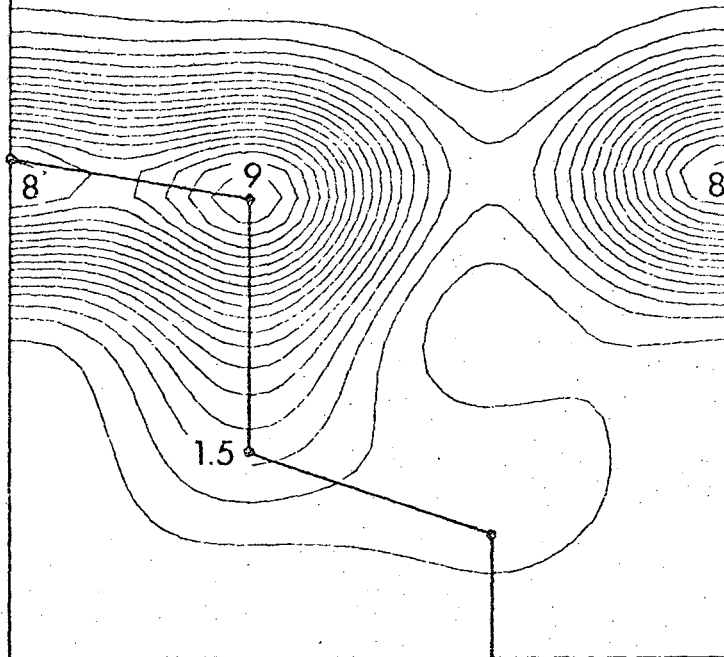
Si (111) SURFACE, RELAXED STATES AT −1.5 eV (Γ_{tb})
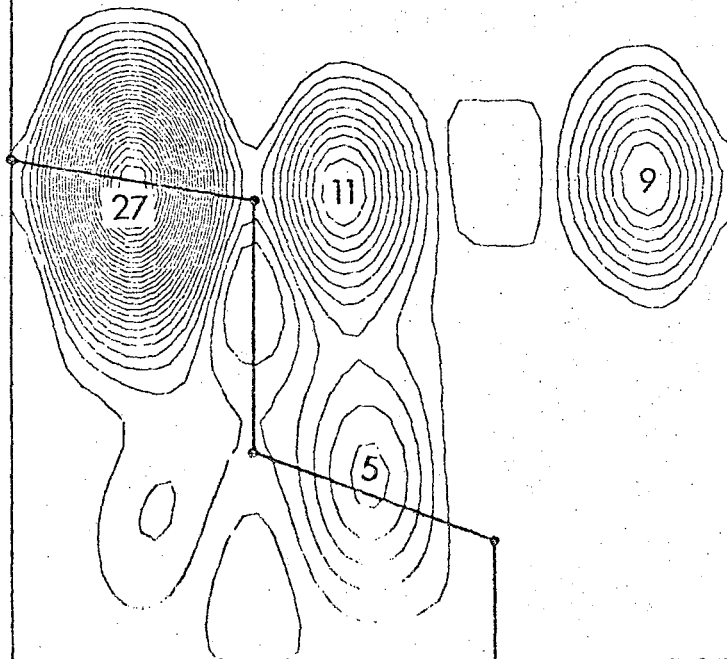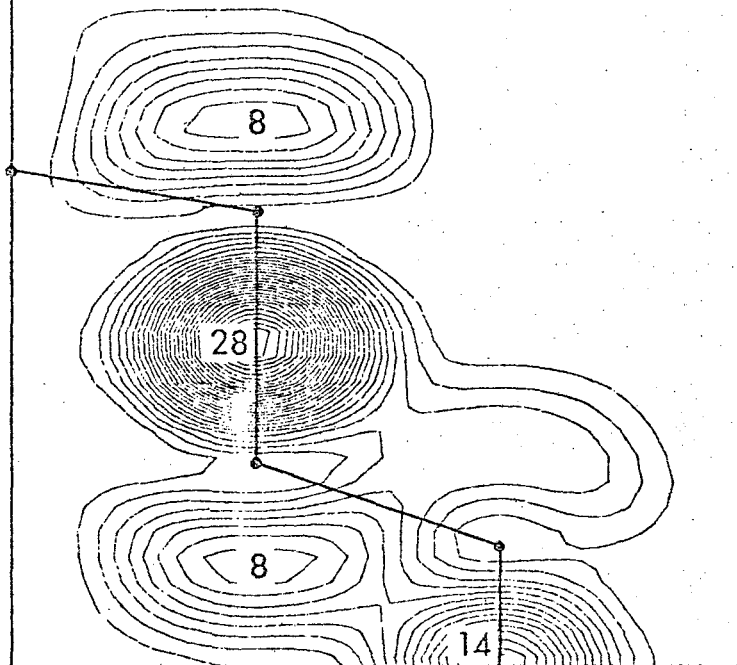
Figure 7

Figure 8

Si (111) surface, relaxed
states at + 0.5 eV (K_d)
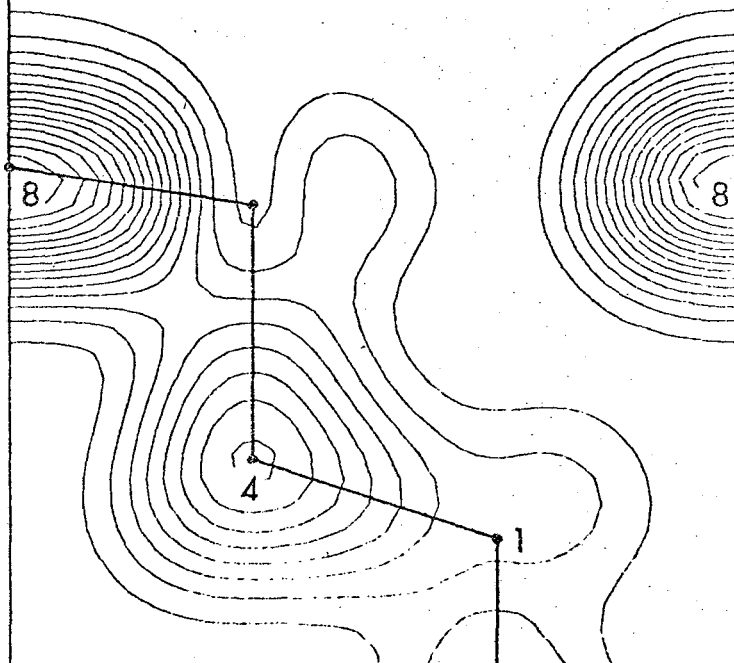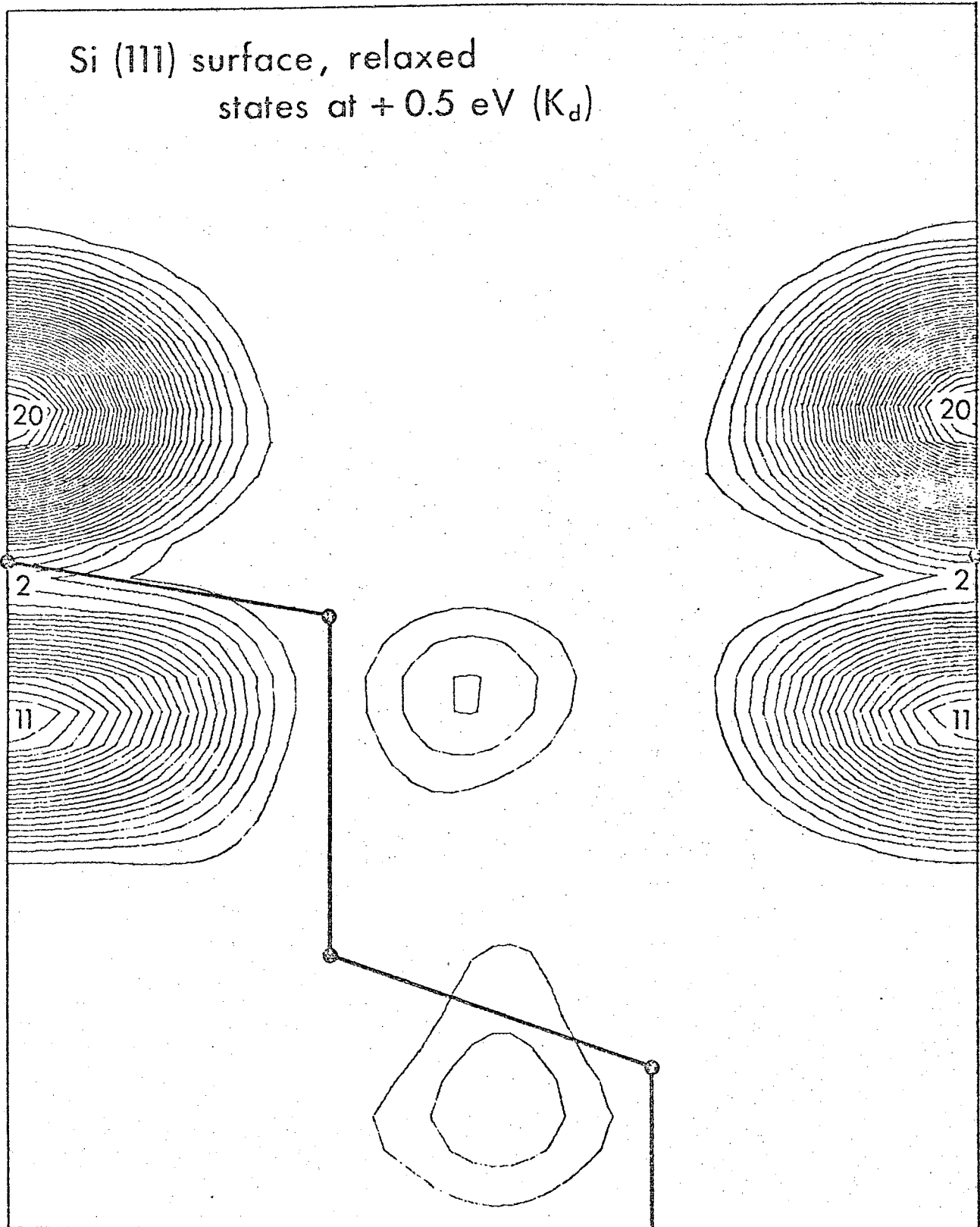
Figure 9

Si (111) — 2 × 1

IDEAL
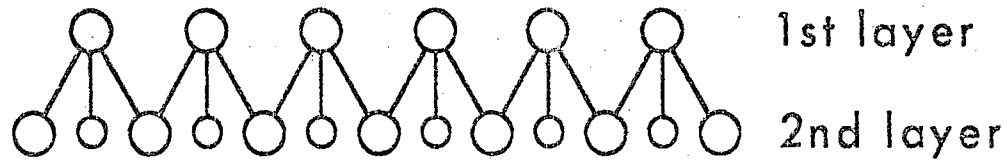
1st layer

2nd layer

HANEMAN'S MODEL

BUCKLED

TOP VIEW

3.84 Å
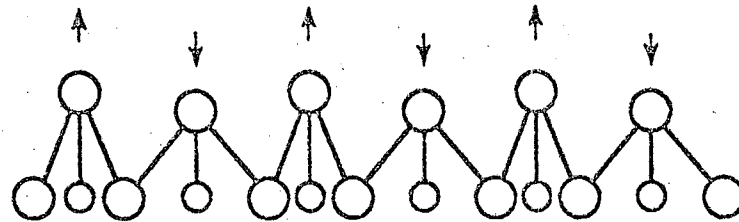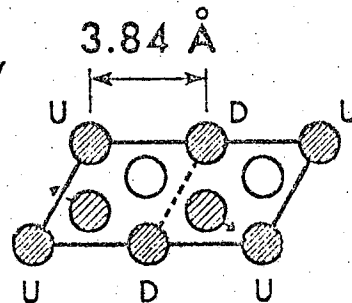
2 × 1

⊘ 1st layer
⊘ 2nd layer
○ 4th layer

Figure 10

Figure 11

Figure 12

Figure 13

0 0 0 0 4 3 0 5 7 6 3